Journal of Power Sources 195 (2010) 6049–6054

Contents lists available at ScienceDirect

Journal of Power Sources

journal homepage: www.elsevier.com/locate/jpowsour

# Effect of slurry preparation process on electrochemical performances of $LiCoO_2$ composite electrode

Gil-Won Lee[a], Ji Heon Ryu[b], Woojoo Han[a], Kyung Hyun Ahn[a], Seung M. Oh[a,*]

[a] Department of Chemical and Biological Engineering and Research Centre for Energy Conversion & Storage, Seoul National University, 56-1, Shilim-dong, Gwanak-ku, Seoul, 151-744, Republic of Korea
[b] Graduate School of Knowledge-Based Technology and Energy, Korea Polytechnic University, Siheung, Gyeonggi, 429-793, Republic of Korea

ARTICLE INFO

*Article history:*
Received 21 October 2009
Received in revised form 7 December 2009
Accepted 24 December 2009
Available online 14 January 2010

*Keywords:*
Li-ion batteries (LIBs)
Rheological properties
Mixing processes
Slurry
Viscosity
Viscoelastic modulus

ABSTRACT

The slurries comprising $LiCoO_2$ powder, carbon, and polymeric binder are prepared by two different mixing processes, and their rheological properties are compared. In the multi-step process, the solvent is added into solid mixture in stepwise, whereas the total amount at once in the one-step process. The former process gives the slurry that is more suitable for electrode preparation with fluid-like behavior and more uniform dispersion of solid ingredients as compared to those prepared from the letter. In the composite electrode prepared from the former, the $LiCoO_2$ and carbon particles are homogeneously distributed without agglomeration. Indebted to this favorable feature, this electrode exhibits a better electrochemical performance for cyclability and rate capability. It is very likely that the contact resistance and charge transfer resistance for lithiation/de-lithiation are smaller in the former electrode due to the homogeneous distribution of $LiCoO_2$ and carbon particles, which leads to a less significant electrode polarization.



## 1. Introduction

At present, the lithium-containing transition metal oxides such as $LiCoO_2$ and $LiMn_2O_4$ are widely used as the positive electrode material for lithium-ion batteries [1,2]. Up to now, however, the major research activities on these materials are primarily focused on their crystal structure, synthesis, doping, surface coating and electrochemical characteristics [3–6]. Commonly, the battery performance is limited by the performance of the constituent materials, such that the above-mentioned fundamental studies and modifications are needed to realize the high-performance batteries. Many reports, however, demonstrated that the battery performances are affected by the other variables such as the nature of carbon additives, polymeric binders, and current collectors, also by the electrode fabrication process.

Until now, the reports on the battery performance studied by employing different electrode fabrication processes are limited [7–13]. Among these, Kim et al. [14] reported that the cell performances are affected by the mixing sequence in the slurry preparation step, in which a solid mixture of electrode material and carbon additive is dispersed in a solution of polymeric binder/solvent. According to their report, a better cycle performance is observed when the slurry is prepared by adding the solution (binder + solvent) in sequence into the pre-mixed solid ingredients (electrode material and carbon additive) as compared to that prepared by adding the solution at once. The better electrode performance observed with the sequential solution addition has been ascribed to a uniform dispersion of solid ingredients in the resulting slurry.

In this work, a detailed study is made on how the sequential addition of solution affects the rheological properties of the slurries such as viscosity, dynamic viscoelastic modulus, and the steady flow properties. To this end, two slurries are prepared by adding the solution either in sequence (multi-step process) or at once (one-step process). To investigate the type of viscosity behavior such as thixotropy, we measure the viscosity as a function of shear rate. Dynamic viscoelastic properties are measured to investigate a degree of flocculation and the type of network structure in the slurries. The steady flow tests are made to address if or not any irreversible structural break-down of solid network occurs in the slurries. After the electrode fabrication from the two slurries, the cross-sectional images are obtained to compare the dispersion of solid ingredients in the two composite electrodes. Electrochemical performances of the resulting $LiCoO_2$ electrodes were compared in terms of cycle performance, cell resistances and rate capability.

* Corresponding author. Tel.: +82 2 880 7074; fax: +82 2 872 5755.
*E-mail address:* seungoh@snu.ac.kr (S.M. Oh).

0378-7753/$ – see front matter © 2010 Elsevier B.V. All rights reserved.
doi:10.1016/j.jpowsour.2009.12.101

## 2. Experimental

### 2.1. Preparation and rheological measurements of the slurries

The slurries were prepared with a $LiCoO_2$ powder (JesEChem, Korea, average particle size = 10 μm, round-shaped), Denka Black (Denka, average particle size = 35 nm) as the conductive additive, and polyvinylidenefluoride (PVdF, Kureha KF-1100, $\bar{M}_w = 7 \times 10^4$) as the binder (95:2.5:2.5 wt. ratio). The solid content ($LiCoO_2$ powder, Denka Black and PVdF) was fixed at 65 wt.% in the slurries. Two different mixing sequences were employed (Fig. 1). In the one-step process, the PVdF and total amount of solvent (*N*-methylpyrrolidinone, NMP, Aldrich) were mixed for 30 min by homogenizer (2000 rpm), into which the $LiCoO_2$ and Denka Black powders pre-mixed in an agitated mortar were added, and mixed for additional 2 h at the same condition. For the multi-step process, the PVdF and two-fifths (in weight) of NMP were mixed in advance. After mixing for 30 min, the pre-mixed solid ingredients were added into this solution. The remaining solvent was then added by dividing into three in every 30 min. The total mixing time was the same (120 min) for two processes.

Rheological properties of the slurries were measured using a stress-controlled rheometer (AR-1500ex, TA Instruments) with a 60 mm diameter cone-and-plate measuring system, with the cone angle 2° and gap of truncated cone tip 56 μm. In order to prevent solvent evaporation during the measurements, a solvent trap was used. Before the measurements, the samples were equilibrated at 23 °C for 10 min in order to remove any previous shear histories and to ensure that the constituent materials establish their equilibrium structures [15]. Steady state flow measurements were made from 100 to 10,000 dyne $cm^{-2}$ to determine the slurry viscosity. For the dynamic viscoelastic measurements, the linear viscoelastic range was determined with stress sweep (0.1–10,000 dyne $cm^{-2}$) at a fixed angular frequency of 1.0 and 100 rad $s^{-1}$, respectively. A frequency sweep was then made by applying a constant oscillation stress of 0.9999 dyne $cm^{-2}$ (one-step process) or 1.9995 dyne $cm^{-2}$ (multi-step process), which were within the linear region, over a frequency range from 0.1 to 628 rad $s^{-1}$ [16]. Steady flow tests were performed to obtain the flow curves (shear rate *vs.* shear stress) and hysteresis loops. The cone was programmed to increase the shear stress from 0.1 to 3000 dyne $cm^{-2}$ (upward flow curve), which was followed by a decrease from 3000 to 0.1 dyne $cm^{-2}$ (downward flow curve).

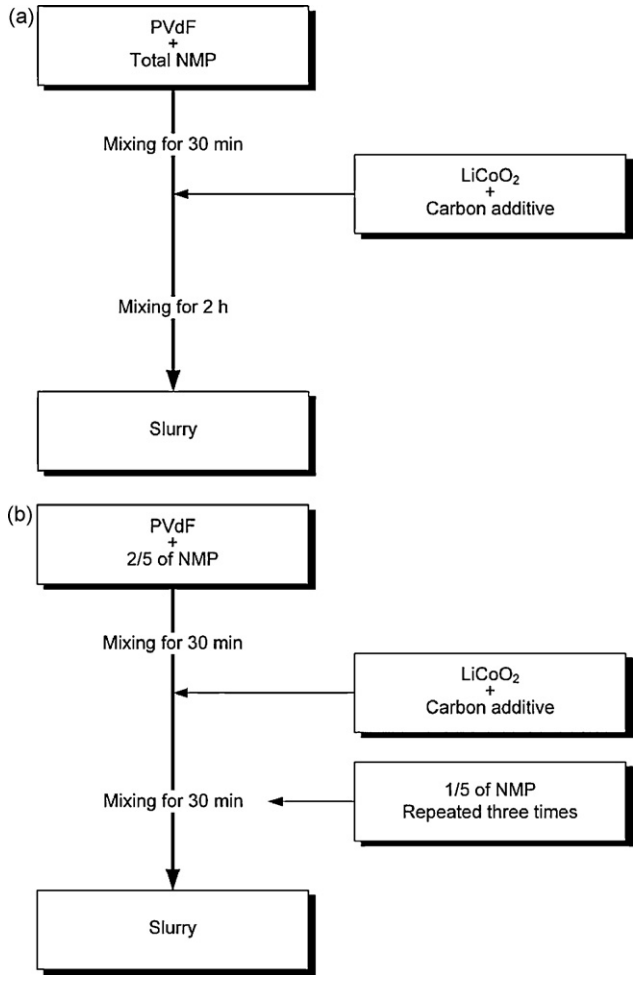


**Fig. 1.** Schematic diagrams for the slurry preparation: (a) one-step process and (b) multi-step process.

### 2.2. Preparation and characterizations of $LiCoO_2$ electrodes

The prepared slurries were coated onto a piece of aluminum foil current collector by using an automatic doctor blade. The electrodes were dried at 120 °C in convection oven for 1 h to evaporate the solvent and pressed through a roll press. Before cell assembly, the electrodes were further dried in a vacuum oven at 120 °C for 12 h. The composite electrodes were crosscut using an argon ion beam (Cross Section Polisher (CP) SM-09010, JEOL) and their field-emission scanning electron microscope (FE-SEM) images and energy dispersive spectroscopy (EDS) elemental mapping were obtained by using a JEOL JSM-7000F.

Coin-type half-cells were assembled with the composite electrode, Li foil as a counter electrode, and polypropylene film as a separator. The used electrolyte was 1.0 M $LiPF_6$ dissolved in a mixture of ethylene carbonate (EC) and ethylmethyl carbonate (EMC) (1:1 vol. ratio), where 1.0 wt.% of vinylene carbonate (VC) was added. The electrodes were fabricated in a dry room (dew point = −50 °C). Electrochemical measurements were made at room temperature using a Toscat-2100 cycler.

In order to measure the area-specific impedance (ASI) as a function of depth of discharge, the hybrid pulse power characterization (HPPC) test was performed, in which the 10-s discharge-pulse and the 10-s charge-pulse resistance at each 10% depth of discharge (DOD) increment were obtained [17]. The test was made up of single repetitions of the test profile (Fig. 2), separated by 10% DOD constant current discharge segments, each followed by 1 h rest period to allow the cell to return to an electrochemical and thermal equilibrium condition before applying the test profile. The test began with a fully charged state after 1 h rest and terminated after completing the final profile at 90% DOD.

## 3. Results and discussion

Fig. 3 presents the viscosity curves (viscosity *vs.* shear rate) of the final slurries prepared by two processes. Both slurries show a shear thinning behavior as judged from the decrease of viscosity with an increase in the shear rate [18]. The viscosity at low shear rates is a measure for the settling behavior of solids and that at high shear rates the processibility [15]. The high viscosity at the low shear rates observed with two slurries is preferred since the settling of solid ingredients is not significant. The low viscosity at the high shear rates observed with two slurries is also a favorable feature because more uniform coating is expected with less viscous slurries. Also, if the latter condition is met, the solvent loading can be minimized in the slurry preparation step.

Even if both slurries show a shear thinning behavior, the slurry prepared by the multi-step process shows better rheological prop-

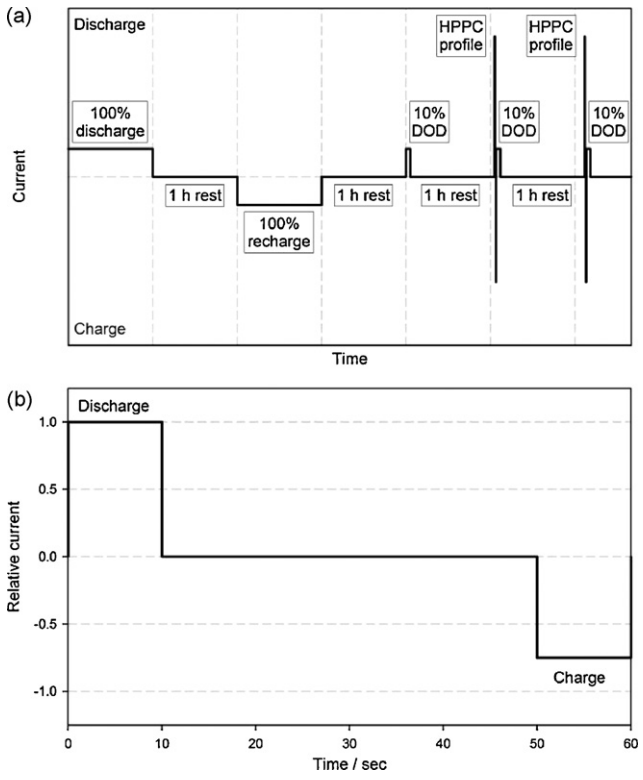


**Fig. 2.** (a) Hybrid pulse power characterization (HPPC) test protocol and (b) the details of the HPPC test profile.

erties. The viscoelastic properties of two slurries are compared in Fig. 4, where two features are immediately apparent. First, the slurry made by the one-step process shows a frequency-independent viscoelastic modulus, which is contrasted by the frequency-dependent behavior with the slurry made by the multi-step process. Second, the storage modulus ($G'$) is larger than the loss modulus ($G''$) in the whole frequency range in the former slurry, whereas the reverse trend is observed with the latter. The frequency-independent viscoelastic moduli with $G' > G''$ strongly indicate that the former slurry is composed of colloidal gel, in which the particulate units are connected together into a volume-filling network structure [18,19]. That is, the solid network structure is not broken, thus the solid ingredients are continuously mixed with a low shear during the mixing. In contrast, the frequency-dependent

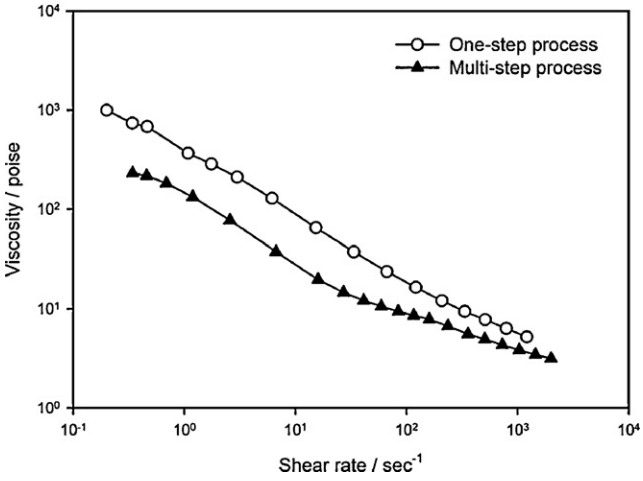


**Fig. 3.** Viscosity of the slurries prepared by two mixing processes against the shear rate.

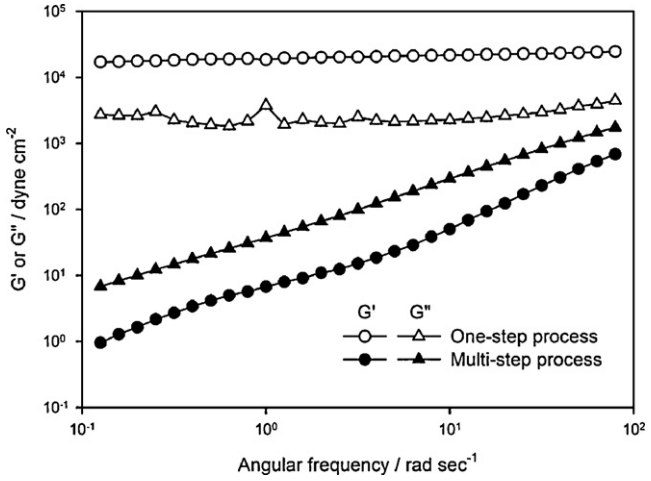


**Fig. 4.** Viscoelastic modulus of the slurries prepared by two mixing processes against the angular frequency.

values with $G' < G''$ reflect that the latter slurry is essentially a low-viscosity sol, in which the particulate units are distinct and separated from one another [20–22]. That is, the network structure is broken.

The break-down of network structure in the latter slurry is further evidenced by the hysteresis flow curves shown in Fig. 5. Hysteresis phenomena were observed in the slurry made by the multi-step process. The shear stress values traced with an increase in shear rates show a difference with those traced by decreasing the shear rate. This is a characteristic feature for the shear-induced break-down of network structures [23,24]. The irreversible structure break-down in the multi-step process seems to be very probable because the mixing starts from a highly viscous state since a smaller amount solvent is added in the initial mixing period. Under these circumstances, the network structure is easily broken as a higher shear rate was applied during the stirring. In contrast, the one-step process starts in a less viscous state because the total amount of solvent is added at once in the initial period.

The slurry made by the multi-step process seems to be rather preferred than that from the one-step process. It is less viscous and the solid ingredients are more uniformly dispersed. To ascertain this, the dispersion of electrode constituents in the electrode

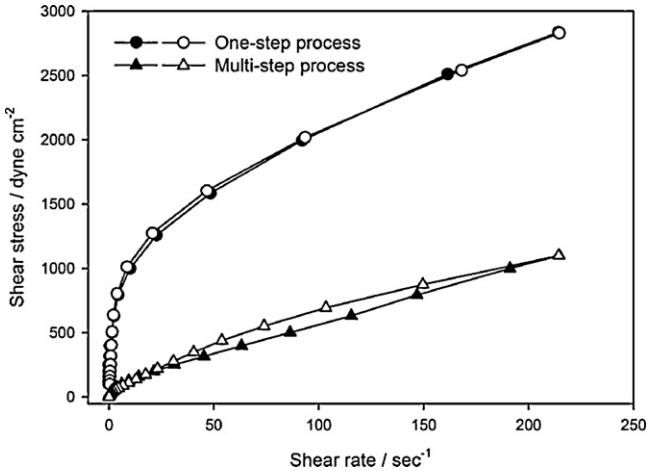


**Fig. 5.** Flow curves of the slurries prepared by two mixing processes. For the measurements, the shear rate was increased in advance, and then decreased. The closed symbols represent the upward flow curves, whereas the open symbols the downward flow curves. The hysteresis loop appears in the slurry prepared by the multi-step process.

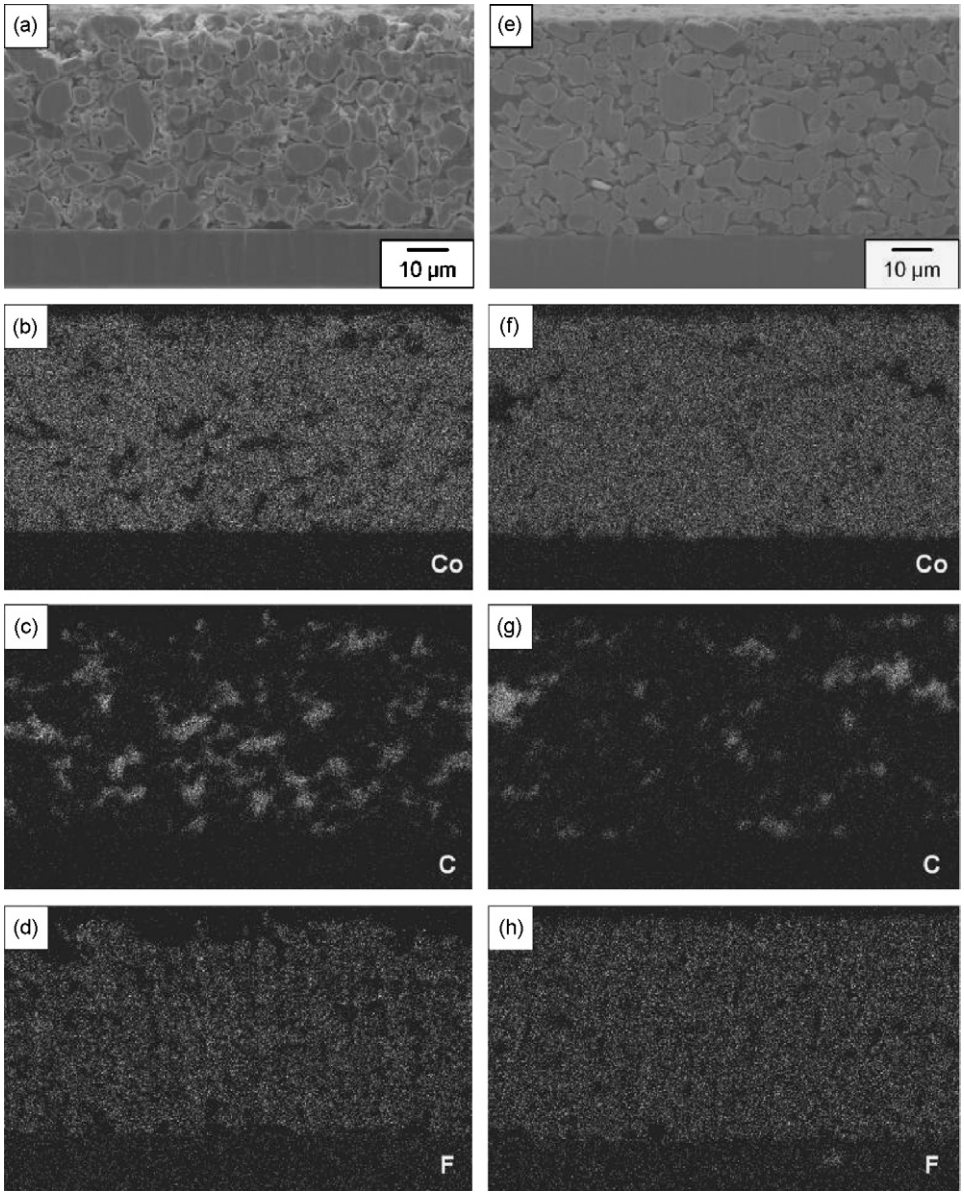


**Fig. 6.** Cross-sectional SEM images of the composite electrodes: (a) from one-step process and (b) from multi-step process. EDS elemental mappings: (b) and (f) cobalt from $LiCoO_2$, (c) and (g) carbon from Denka Black and PVdF, and (d) and (h) fluorine from PVdF.

layer is analyzed. Fig. 6 shows the cross-sectional images of the electrode layer obtained by FE-SEM. The comparison for Fig. 6a and e reveals that the electrode layer fabricated from the slurry made by the multi-step process is more compact and the dispersion is more homogenous as compared to that derived from the one-step process. The EDS dot images further confirm this feature. The Co mapping obtained with the former electrode (Fig. 6f) indicates that the lighter dots corresponding to the Co atoms ($LiCoO_2$) are uniformly distributed. In the case of the latter electrode, however, there appear darker spots. The darker spots must come from the carbon additive (Denka Black) as evidenced by the carbon mapping. The lighter dot images in Fig. 6c and g coincide with the darker spots in Fig. 6b and f, ensuring that the darker spots in Fig. 6b and f come from the carbon additive. Clearly, the solid ingredients are more uniformly dispersed in the electrode prepared by the multi-step mixing. In the other electrode, however, some carbon particles are agglomerated instead of uniform dispersion.

The cycle performance of two electrodes is compared in Fig. 7. A larger capacity loss is observed with the electrode prepared by the one-step process. In this electrode, only 60% of the initial capacity is retained in the 70th cycle, which is lower than that observed with the electrode prepared by the multi-step process (70%). The capacity fading seems to be higher than that observed in commercial cells. This may be due to the fact that the electrodes were charged up to 4.3 V (*vs.* $Li/Li^+$), under which circumstances the phase transition may take place in $LiCoO_2$. Also, the oxidative electrolyte decomposition may take place on the electrode surface. The phase transition and electrolyte decomposition may be suppressed by doping or surface coating. But the used $LiCoO_2$ was not modified in such ways.

The reason why the electrode made by the one-step process shows a poorer cycle performance can be accounted for by comparing the evolution of cell resistances. The cell resistances for discharging and charging were monitored as a function of depth of discharge (DOD) (Fig. 8). The area-specific impedances (ASI) were determined using a $\Delta V/I$ calculation for each iteration employing the HPPC test protocol. Two features should be noted in Fig. 8. First, the cell resistance for discharging (discharge resistance) is larger

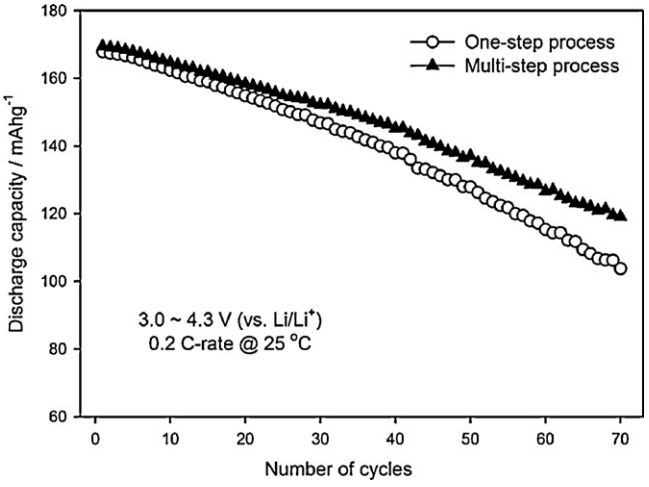


**Fig. 7.** Discharge capacity observed with the $Li/LiCoO_2$ cells according to the cycle number. The galvanostatic charge–discharge cycling was made at a constant current (0.2*C* rate) between 3.0 and 4.3 V (*vs.* $Li/Li^+$).

than the charge resistance, particularly at the end of discharge. Generally, the resistance for discharge (lithiation in the case of positive electrode) is larger than the charge resistance since the $Li^+$ insertion into solid lattices is kinetically slower than $Li^+$ extraction [25,26]. Also, the lithiation resistance becomes larger at the end of discharge since the available $Li^+$ storage sites become scarce. This

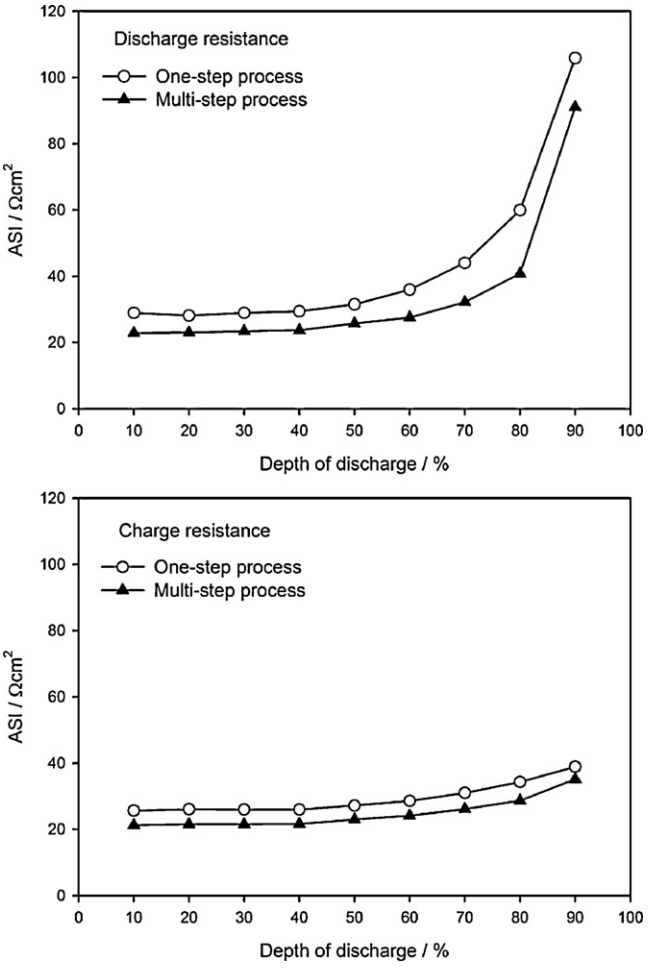


**Fig. 8.** Area-specific impedances (ASI) for discharging and charging that were traced a function of depth of discharge.

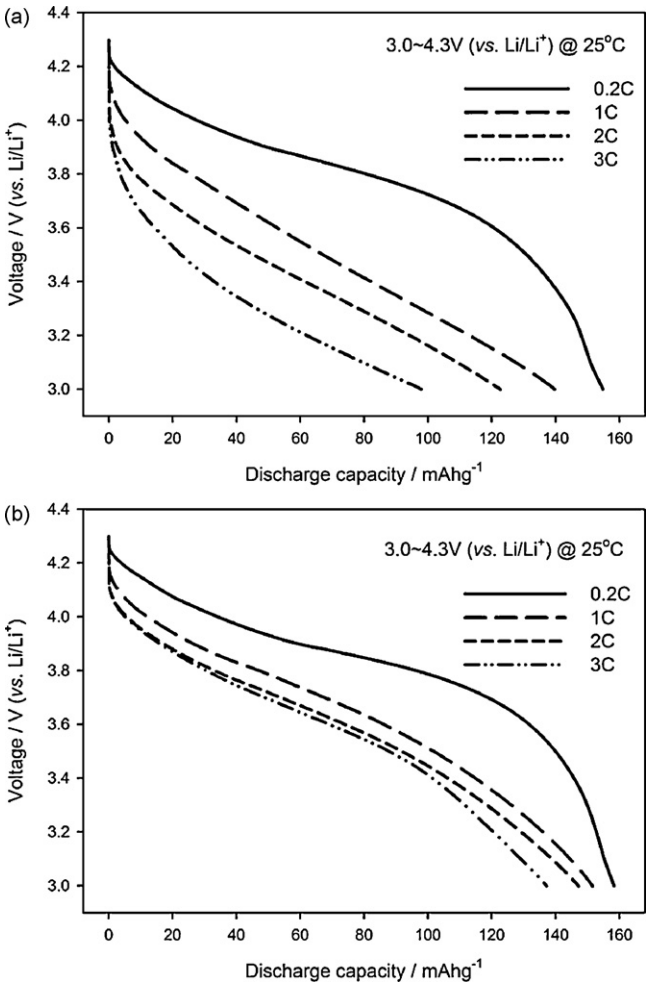


**Fig. 9.** Galvanostatic discharge voltage profiles observed with the $Li/LiCoO_2$ cells: (a) from one-step process and (b) from multi-step process. The charging was made at a constant current (0.2*C* rate), whereas the discharging was made at four different rates (0.2*C*, 1*C*, 2*C* and 3*C*).

is what the results in Fig. 8 illustrate. The second observation in Fig. 8 is that both the discharge and charge resistance are smaller in the electrode fabricated by the multi-step process. In order to compare the cell resistance for two electrodes, the galvanostatic discharge profiles were traced as a function of current in Fig. 9. The electrode made by the one-step process (Fig. 9a) shows an ever-increasing electrode polarization with an increase in the discharge current. Such an electrode polarization is, however, less significant in the electrode prepared by the multi-step process (Fig. 9b). This behavior can be explained on the basis of the dispersion of solid ingredients in the slurries. The multi-step process gives more uniform dispersion of $LiCoO_2$ and Denka Black particles in the slurry (Fig. 4), which in turn allows more uniform dispersion of the solids in the composite electrode layer (Fig. 6). Indebted to this favorable feature, both the contact resistance between the $LiCoO_2$ and Denka Black particles, and the charge transfer resistance for lithiation/delithiation are smaller in this electrode (Fig. 8). The smaller internal resistance (sum of contact and charge transfer resistance) leads to a less severe electrode polarization (Fig. 9) and eventually to a better cycle performance (Fig. 7).

## 4. Conclusion

The homogeneity of solid dispersion was compared for two slurries made by two different mixing processes. The electrochem-

ical performances for the $LiCoO_2$ composite electrodes prepared from the two slurries were also compared with respect to the dispersion of electrode materials in the electrode layer, electrode resistance and cycle retention. The following points of value may be gleaned.

(i) Even if the final solid loading is the same for the two slurries, the rheological properties are different according to the mixing process. The slurry made by the one-step process is composed of colloidal gel, in which the powder units are connected inside a volume-filling network structure, thereby giving rise to a solid-like behavior with higher viscosity. In contrast, the slurry made by the multi-step process is essentially a low-viscosity sol, in which the particulate units are distinct and separated from one another. Such a break-down of network structure takes place because the mixing in the initial period starts from a highly viscous state as the solvent loading is smaller. Under these circumstances, the network structure is easily broken since a higher shear rate is applied for mixing.
(ii) In the composite electrode prepared by the multi-step process, the $LiCoO_2$ and carbon particles are more uniformly distributed. As a result, the electrode polarization is less significant, leading to a better cycling and rate capability.

## Acknowledgements

This work was supported by the WCU program through KOSEF funded by the Ministry of Education, Science and Technology (400-2008-0230). The authors also wish to acknowledge the Research Center for Energy Conversion and Storage for financial support.

## References

[1] K.M. Abraham, D.M. Pasquariello, E.M. Willstaedt, J. Electrochem. Soc. 145 (1998) 482–486.
[2] G.B. Appetecchi, B. Scrosati, Electrochim. Acta 43 (1998) 1105–1107.
[3] J.N. Reimers, J.R. Dahn, J. Electrochem. Soc. 139 (1992) 2091–2097.
[4] G.G. Amatucci, J.M. Tarascon, L.C. Klein, Solid State Ionics 83 (1996) 167–173.
[5] Z. Chen, J.R. Dahn, Electrochem. Solid-State Lett. 5 (2002) A213–A216.
[6] J. Cho, Y.J. Kim, B. Park, J. Electrochem. Soc. 148 (2001) A1110–A1115.
[7] R. Dominko, M. Gaberscek, J. Drofenik, M. Bele, S. Pejovnik, Electrochem. Solid-State Lett. 4 (2001) A187–A190.
[8] D. Guy, B. Lestriez, R. Bouchet, D. Guyomard, J. Electrochem. Soc. 153 (2006) A679–A688.
[9] E. Ligneel, B. Lestriez, O. Richard, D. Guyomard, J. Phys. Chem. Solids 67 (2006) 1275–1280.
[10] M. Yoo, C.W. Frank, S. Mori, Chem. Mater. 15 (2003) 850–861.
[11] M. Yoo, C.W. Frank, S. Mori, S. Yamaguchi, Chem. Mater. 16 (2004) 1945–1953.
[12] C.-C. Li, J.-T. Lee, X.-W. Peng, J. Electrochem. Soc. 153 (2006) A809–A815.
[13] E. Ligneel, B. Lestriez, A. Hudhomme, D. Guyomard, J. Electrochem. Soc. 154 (2007) A235–A241.
[14] K.M. Kim, W.S. Jeon, I.J. Chung, S.H. Chang, J. Power Sources 83 (1999) 108–113.
[15] S.R. Raghvan, S.A. Khan, J. Rheol. 39 (1995) 1311–1325.
[16] S.R. Raghavan, M.W. Riley, P.S. Fedkiw, S.A. Khan, Chem. Mater. 10 (1998) 244–251.
[17] Idaho National Laboratory, Battery test manual for Plug-in hybrid electric vehicles, INL/EXT-07-12536, March 2008, pp. 3–42.
[18] T.G. Mezger, The Rheological Handbook: For Users of Rotational and Oscillation Rheometers, first ed., Vincentz Verlag, Hannover, 2002, pp.16–85, 112–163.
[19] S.R. Raghavan, J. Hou, G.L. Baker, S.A. Khan, Langmuir 16 (2000) 1066–1077.
[20] S.R. Raghavan, S.A. Khan, J. Colloid Interface Sci. 185 (1997) 57–67.
[21] D.T. Atkins, B.W. Ninham, Colloids Surf. 129 (1997) 23–32.
[22] H.J. Walls, S.A. Khan, Langmuir 16 (2000) 7920–7930.
[23] D.A. Williams, A.W. Saak, H.M. Jennings, Cement Concrete Res. 29 (1999) 1491–1496.
[24] T.H. Kim, L.W. Jang, D.C. Lee, H.J. Choi, M.S. Jhon, Macromol. Rapid Commun. 23 (2002) 191–195.
[25] C.Y. Yao, T.H. Kao, C.H. Cheng, J.M. Chen, W.M. Hurng, J. Power Sources 54 (1995) 491–493.
[26] H. Sato, D. Takahashi, T. Nishina, I. Uchida, J. Power Sources 68 (1997) 540–544.